# Shapiro Steps in Driven Atomic Josephson Junctions

Vijay Pal Singh,[1] Juan Polo,[1] Ludwig Mathey,[2,3] and Luigi Amico[1,4,5]
[1]Quantum Research Center, Technology Innovation Institute, Abu Dhabi, United Arab Emirates
[2]Zentrum für Optische Quantentechnologien and Institut für Quantenphysik, Universität Hamburg, 22761 Hamburg, Germany
[3]The Hamburg Center for Ultrafast Imaging, Luruper Chaussee 149, Hamburg 22761, Germany
[4]INFN-Sezione di Catania, Via S. Sofia 64, 95127 Catania, Italy
[5]Dipartimento di Fisica e Astronomia, Università di Catania, Via S. Sofia 64, 95123 Catania, Italy

(Received 21 July 2023; revised 22 December 2023; accepted 26 June 2024; published 26 August 2024)

We study driven atomic Josephson junctions realized by coupling two two-dimensional atomic clouds with a tunneling barrier. By moving the barrier at a constant velocity, dc and ac Josephson regimes are characterized by a zero and nonzero atomic density difference across the junction, respectively. Here, we monitor the dynamics resulting in the system when, in addition to the above constant velocity protocol, the position of the barrier is periodically driven. We demonstrate that the time-averaged particle imbalance features a plateau behavior that is the analog of Shapiro steps observed in driven superconducting Josephson junctions. The underlying dynamics reveals an intriguing interplay of the vortex and phonon excitations, where Shapiro steps are induced via suppression of vortex growth. We study the system with a classical-field dynamics method, and benchmark our findings with a driven circuit dynamics.

DOI: 10.1103/PhysRevLett.133.093401

Superconducting Josephson junctions (JJs) exhibit a transition between the dc and ac Josephson effect by developing a dc voltage when the current exceeds a critical value [1]. In the presence of microwave radiation driving the junction, characteristic dc-ac transitions can occur as a result of photon-assisted tunneling processes. Accordingly, for an averaged voltage matching multiples of the driving frequency, the supercurrent jumps between different "dc plateaus," reflecting that the Cooper pairs' phase change is effectively synchronized with the external ac source [2]. The resulting steps displayed in the I-V characteristics are referred to as Shapiro steps [3,4]. Such picture has been confirmed with experiments carried out on driven superconducting JJs [5–7]. Shapiro steps play an important role both for the fundamental understanding of superconductivity and practical applications of JJs, such as metrological voltage standards [8–10].

Similarly to the dc and ac Josephson effects in superconducting junctions, dissipationless-viscous transitions can occur also in neutral $^3$He and $^4$He quantum fluids flowing through suitable constrictions. This phenomenon has been demonstrated to result from phase slips nucleating in the hydrodynamical field [11–14]. By suitable driving of the pressure across the constriction, a matter flow with Shapiro-type step behavior was reported in superfluid $^3$He [15].



Ultracold atoms have emerged as ideal systems to implement and study atomtronic analogs of superconducting circuits [16–24]. Atomic Josephson junctions (JJs) were realized using weak links of atom clouds [25–28], enabling the study of important effects as macroscopic self-trapping [29] and current-phase relation [30,31]. Following the seminal paper of Giovannazzi *et al.* [32], the Josephson effect in ultracold atom systems can be studied by moving a barrier separating two degenerate gas clouds at rest. An analog of a dc to ac Josephson response occurs in which the difference of the particle densities of the two sides of the junction (termed as particle imbalance throughout the manuscript) changes from zero to a finite value. The current-chemical potential (playing the role of the voltage in superconducting JJ) relation was achieved in a series of remarkable experiments [31,33,34]. Such a behavior can be captured by a resistively and capacitively shunted junction (RCSJ) circuit model [35]. Phase-slip induced dissipation was studied in Refs. [36–40]. Theoretically, Josephson effects were studied using a two-mode Gross-Pitaevskii equation model [32,41,42]. Even though specific resonances were noticed in periodically tilted double wells, experimentally feasible protocols to realize Shapiro steps in condensates have not been provided yet [42–45].

With the remarkable progress in dynamical light shaping achieved recently [46–48], driven matter-wave circuits are well within the experimental capabilities. Here, we consider a driven JJ: while moving the barrier with a velocity $v$, we drive its position periodically; see Fig. 1(a). With this, we observe that the dynamics of the system features steps of the Shapiro type that manifest themselves

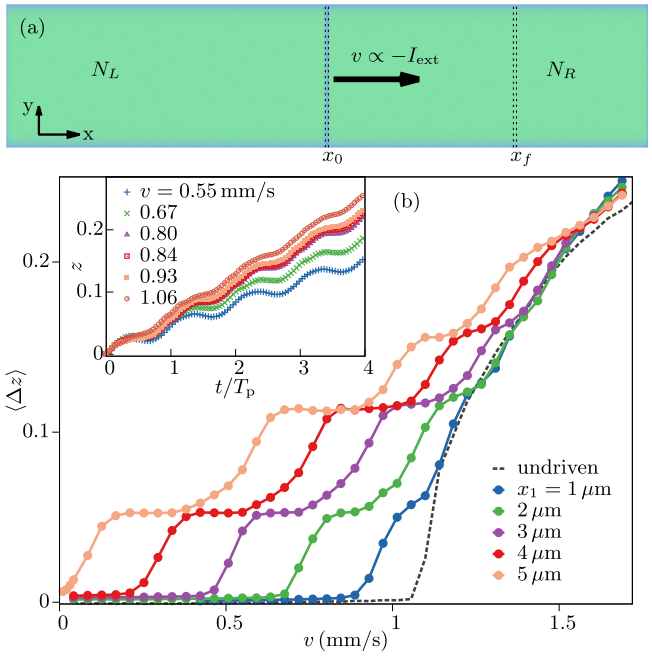


FIG. 1. Atomic Josephson junction and emergence of Shapiro steps. (a) Simulation of a Josephson junction consisting of two clouds separated by a tunneling barrier of height $V_0$ and width $w$. The barrier is moved at constant velocity $v$ (arrow) from the position $x_0$ until the final position $x_f$, which induces an external current $I_{\rm ext}$. In addition, we modulate the barrier location using the protocol $x(t) = vt + x_1 \sin(2\pi f t)$, where $f$ is the frequency and $x_1$ is the amplitude of driving. $N_L$ ($N_R$) represents the atom number of the left (right) reservoir. (b) Imbalance $\Delta z = z - \bar{z}$ as a function of $v$ for the undriven case (dashed line). $\bar{z}$ is the equilibrium imbalance determined at $x_f$ that varies with $v$. Time-averaged imbalance $\langle \Delta z \rangle$ shown for $f = 45$ Hz and $x_1 = 1$, 2, 3, 4, and 5 μm. Inset shows the time evolution of $z(t)$ at different $v$ for the driving with $x_1 = 3$ μm, where $T_{\rm p} = 1/f$ is the driving period. We use the barrier height $V_0/\mu = 1.5$, where $\mu$ is the mean-field energy.

as a time-averaged atom imbalance; see Fig. 1(b). We demonstrate how the observed dynamics is controlled by specific features of phonon excitations and vortex nucleation. The results are obtained by classical-field methods that include fluctuating bosonic fields beyond mean-field description [49–52]. We benchmark our results with the dynamics of a driven RCSJ circuit model.

*System and method*—We simulate the dynamics of a generic condensate of bosons using classical-field dynamics within the truncated Wigner approximation [49–52]. We consider a homogeneous cloud of bosons confined in a box of dimensions $L_x \times L_y$. The system is described by the Hamiltonian

$$\hat{H}_0 = \int d\mathbf{r} \left[ \frac{\hbar^2}{2m} \nabla\hat{\psi}^\dagger(\mathbf{r}) \cdot \nabla\hat{\psi}(\mathbf{r}) + \frac{g}{2}\hat{\psi}^\dagger(\mathbf{r})\hat{\psi}^\dagger(\mathbf{r})\hat{\psi}(\mathbf{r})\hat{\psi}(\mathbf{r}) \right]. \quad (1)$$

$\hat{\psi}$ ($\hat{\psi}^\dagger$) is the bosonic annihilation (creation) operator. The interaction $g = \tilde{g}\hbar^2/m$ is given in terms of the dimensionless parameter $\tilde{g} = \sqrt{8\pi} a_s/\ell_z$, where $m$ is the mass, $a_s$ is the $s$-wave scattering length, and $\ell_z = \sqrt{\hbar/(m\omega_z)}$ is the harmonic oscillator length in the transverse direction. Within the classical-field representation we replace the operators $\hat{\psi}$ in Eq. (1) and the equations of motion by complex numbers $\psi$. The initial states $\psi(\mathbf{r}, t = 0)$ are sampled in a grand canonical ensemble with chemical potential $\mu$ and temperature $T$ via a classical Metropolis algorithm [53]. The resulting distribution provides the fluctuations of $\psi(\mathbf{r}, t = 0)$ around its mean-field value. Finally, each initial state is propagated using the equations of motion

$$i\hbar\dot{\psi}(\mathbf{r}, t) = \left( -\frac{\hbar^2}{2m}\nabla^2 + V(\mathbf{r}, t) + g|\psi|^2 \right)\psi(\mathbf{r}, t), \quad (2)$$

which include the barrier potential given by $V(\mathbf{r}, t) = V_0(t)\exp[-2(x - x(t))^2/w^2]$. $V_0(t)$, $w$ and $x(t)$ are the barrier's strength, width, and location. For numerical calculations, we discretize space on a lattice of size $N_x \times N_y$ and a discretization length $l = 0.5$ μm. While we present our results for the concrete realization provided by $^6Li_2$ molecules, we emphasize that our protocol can be applied to any cold-atom degenerate gas. We choose the density $n \approx 5.6\ \mu\text{m}^{-2}$, $\tilde{g} = 0.1$, $T/T_0 = 0.06$, and $L_x \times L_y = 512 \times 27\ \mu\text{m}^2$. The critical temperature $T_0$ is estimated by $T_0 = 2\pi n\hbar^2/(mk_{\rm B}\mathcal{D}_c)$, where $\mathcal{D}_c = \ln(380/\tilde{g})$ is the critical phase-space density [56,57]. We use $w/\xi = 1.1$ and $V_0$ in the range $V_0/\mu \equiv \tilde{V}_0 = 1$–4, where $\xi = \hbar/\sqrt{2mgn}$ is the healing length and $\mu = gn$ is the mean-field energy. To create the weak link at the location $x(t) = x_0 = L_x/2$, we ramp up $V_0$ linearly over 200 ms and wait for 50 ms. Following [31,32], the Josephson current can be obtained by moving the barrier at a constant velocity $v$ until it reaches the final position $x_f$, as depicted in Fig. 1(a). Here, we will discuss the dynamics of the system obtained when the barrier features a periodic driving in addition to its motion with constant velocity,

$$x(t) = vt + x_1 \sin(2\pi f t), \quad (3)$$

where $x_1$ is the amplitude and $f$ is the frequency of driving. We calculate the atom number $N_L(t)$ [$N_R(t)$] in the left (right) reservoir to determine the imbalance $z(t) = [N_L(t) - N_R(t)]/N$, where $N = (N_L + N_R)$ is the total atom number. The barrier motion induces an external current given by $I_{\rm ext}(t) = (\bar{z}N/2) \times |v|/\Delta x$, where $\Delta x$ is the displacement and $\bar{z}$ is the equilibrium imbalance at the final location $x_f = x_0 + \Delta x$. Throughout the Letter we fix the driving time $t_f$ to four cycles. We calculate $z(t)$ for various values of $v$; see inset of Fig. 1(b). By fitting $z(t)$ with a linear function we obtain the value of the time-averaged imbalance

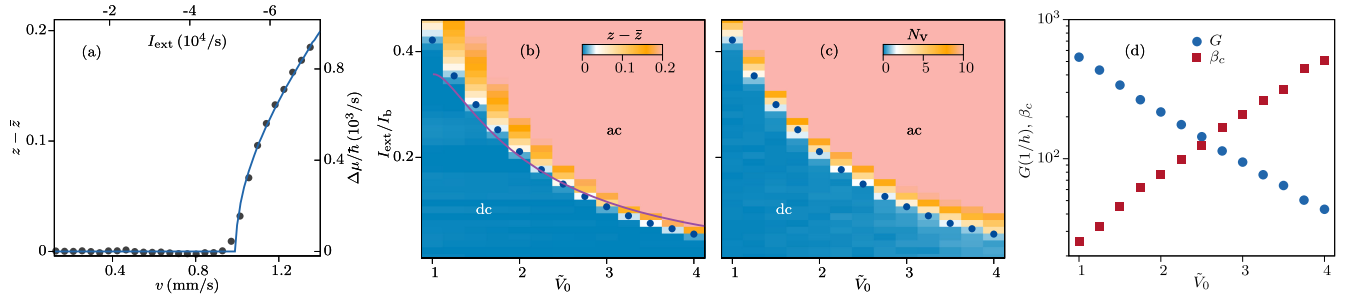


FIG. 2. Characterizing an atomic Josephson junction. (a) Imbalance $z-\bar{z}$ as a function of $v$ for $\tilde{V}_0 = 1.5$ (dots) and its correspondence to the current-chemical potential results (second axes). We fit the response with $\langle\Delta\mu\rangle = \sqrt{I_{\rm ext}^2 - I_c^2}/G$ (continuous line) to determine the critical current $I_c$ and the conductance $G$. (b) $z-\bar{z}$ as a function of $\tilde{V}_0$ and $I_{\rm ext}/I_{\rm b}$, where $I_{\rm b}$ is the bulk current. The results of $I_c$ (dots) are compared with the theoretical prediction $I_{c,\rm p}$ (continuous line); see text. (c) Total vortex number $N_{\rm v}$ determined from the same simulations as in (b), which shows a sharp onset of vortex growth above $I_c$ (dots). (d) Conductance $G$ (dots) and Stewart-McCumber parameter $\beta_c$ (squares) determined for $\tilde{V}_0$ in the range 1–4.

$\langle\Delta z\rangle$ at $t_f$, where $\langle\Delta z\rangle = \langle z\rangle - \bar{z}(x_f)$ with $x_f = |v| \times t_f$. $\langle..\rangle$ refers to the time-averaged response throughout the Letter. In Fig. 1(b), the driven response shows the formation of Shapiro steps in comparison to the undriven system, which we explain below. For the undriven case, we show $\Delta z = z - \bar{z}(x_f)$ determined at the same $t_f$ as the driven case. We quantify the change in the chemical potential $\Delta\mu = NE_c\Delta z/2$, where $E_c = 4(\partial\mu/\partial N)$ is the effective charging energy.

*Characterization of the dc-ac regimes*—We first introduce the driven RCSJ model and then analyze the dc-ac regimes of the undriven junction. We note that this is intrinsically different from the two-mode Gross-Pitaevskii equations, which converge to the RCSJ model in the ideal underdamped limit only. The RCSJ model is a lumped elements circuit to model the dynamics of JJs [35]. The Kirchhoff law of the driven RCSJ circuit reads

$$I_{\rm ext} + I_1\tilde{\omega}\cos(\omega t) = I_c\sin\phi - G\Delta\mu - C\Delta\dot{\mu}, \qquad (4)$$

where $I_c$ is the critical current, $\phi = \phi_L - \phi_R$ the phase difference across the junction, $G$ the conductance, and $C = 1/E_c$ the capacitance. The Josephson relation for the phase dynamics is $\hbar\dot{\phi} = -\Delta\mu$, meaning that $\Delta\mu$ plays the role of the voltage across the junction. $I_1\tilde{\omega}$ is the amplitude and $\omega$ is the frequency of ac drive, with $\tilde{\omega} = \omega/\omega_{\rm J}$, where $\omega_{\rm J} = \sqrt{I_cE_c/\hbar}$ is the Josephson frequency. By using the expression of $\Delta\mu$ we provided above, the circuit is described as an effective driven resistively shunted junction model

$$\dot{z}N/2 + I_1\tilde{\omega}\cos(\omega t) = I_c\sin\phi + \hbar G\dot{\phi}. \qquad (5)$$

The undriven case (i.e., $I_1 = 0$) is solved analytically, yielding the time-averaged chemical potential $\langle\Delta\mu\rangle = G^{-1}\sqrt{I_{\rm ext}^2 - I_c^2}$, which we use to fit our results for the $\Delta\mu(I_{\rm ext}, t_f)$ curve. Based on this fit, we determine $I_c$ and $G$. Here, for the undriven case, we use the constant displacement of $\Delta x = 150$ μm, which results in the same equilibrium imbalance $\bar{z} = 0.59$ at $x_f$ for all $v$. As shown in Fig. 2(a), there is a nonzero $\Delta\mu$ only when $I_{\rm ext}$ exceeds $I_c$, which marks the transition from the dc to ac Josephson effect. The junction becomes resistive with a finite $\Delta\mu$ above $I_c$. We map out the ac resistive regime for a wide range of $\tilde{V}_0$ in Fig. 2(b). The onset of the resistive regime occurs at a low value of $I_c$ for high $\tilde{V}_0$. We compare the results of $I_c$ with the predictions of the critical current $I_{c,\rm p} = I_{\rm b}t_0(\tilde{V}_0, w)$ derived for an ideal Josephson junction [37]. The bulk current $I_{\rm b} = cn_0L_y$ is determined using the sound velocity $c = \sqrt{gn/m}$ and the condensate density $n_0$. We use the variational solution of the tunneling amplitude $t_0(\tilde{V}, d)$ obtained across a rectangular barrier of width $d$ and height $\tilde{V}$ [37], with $d \approx 1.1w$ and $\tilde{V} = \tilde{V}_0$ [53]. In Fig. 2(b) the results of $I_{c,\rm p}$ show good agreement with the simulation results.

To characterize the resistive regime, we study the dynamics of the condensate's local density and phase. While we observe no distinctive change in the dynamics for $I_{\rm ext}$ below $I_c$, characteristic density patterns due to phonon and vortex excitations, resulting in an increase of the imbalance, occur for $I_{\rm ext}$ above $I_c$ [53]. We identify vortex excitations by calculating the phase winding around the lattice plaquette of size $l \times l$ using $\sum_\square \delta\theta(x,y) = \delta_x\theta(x,y) + \delta_y\theta(x+l,y) + \delta_x\theta(x+l,y+l) + \delta_y\theta(x,y+l)$, where $\theta(x,y)$ is the phase field of $\psi(x,y)$ and the phase differences between sites are taken to be $\delta_{x/y}\theta(x,y) \in (-\pi,\pi]$. We associate a vortex (an antivortex) by a phase winding of $2\pi$ ($-2\pi$). By counting all vortices and antivortices we determine the total vortex number $N_{\rm v}$ and average it over the initial ensemble. Figure 2(c) shows a rapid growth of $N_{\rm v}$ above $I_c$ and no vortex excitation below $I_c$. This confirms that the energy in the resistive regime is dissipated by the creation of vortex-antivortex pairs, which is analogous to phase slips in $^4$He [11,12] and atomic weak links [36].

In Fig. 2(d), we demonstrate that the dependence of both the conductance $G$ and the Stewart-McCumber parameter $\beta_c = I_c C/(\hbar G^2)$ is consistent with an exponential dependence on $\tilde{V}_0$. The characteristic dependence between $G$ and $I_c$ yields to $G \propto I_c^{\alpha}$, with $\alpha = 1.2$ [53], resembling the linear dependence of the Ambegaokar-Baratoff relation [54]. The values of $\beta_c$ are in the range between 25 and 500, which fulfills the junction dynamics being in the underdamped regime ($\beta_c \gg 1$). The dependence of $\beta_c$ on $G$ follows the behavior $\beta_c \propto G^{-1.17}$ [53].

*Driven response and Shapiro steps*—We now turn to the dynamics of a periodically driven junction, which is obtained using the barrier protocol described in Eq. (3); see also Fig. 1(a). In Fig. 3(a) the time-averaged response of $\langle \Delta\mu \rangle$ features the creation of regular steps occurring at $\langle \Delta\mu \rangle = khf$, where $k$ is an integer denoting the step index. The onset current location and width of the step vary according to the value of $x_1$. To benchmark our results we numerically solve the driven RCSJ model and analyze its time-averaged response for various parameters, where the current-driving amplitude $I_1$ is related to $x_1$ via $x_1 = I_1 v_c/(I_c \omega_J)$ in which $v_c$ is the critical velocity associated with $I_c$ [53]. The results of the driven model confirm the formation of the Shapiro steps at $\langle \Delta\mu \rangle = khf$ in agreement with our simulations; see Fig. 3(b). The steps obtained by the driven RCSJ model are smoothed out due to the thermal fluctuations of the initial state and a driving-induced depletion of the condensate density. As a result, especially for $k > 2$, the steps are obtained with a specific broadening and amplitude suppression.

Below, we monitor the formation of vortices taking place while the system is driven. Figure 3(c) shows the total number $\langle N_v \rangle$ of vortices nucleating during driving, averaged over two driving cycles [53]. Remarkably, $\langle N_v \rangle$ features a similar plateau structure as the $\langle \Delta\mu \rangle$ response: $\langle N_v \rangle$ increases rapidly at the onset of the steps and undergoes a suppressed vortex nucleation during the steps formation. For $x_1 = 5$ μm, $\langle N_v \rangle$ shows a distinct behavior compared to the results at lower $x_1$. $\langle N_v \rangle$ starts out with a nonzero value undergoing a plateau structure during the

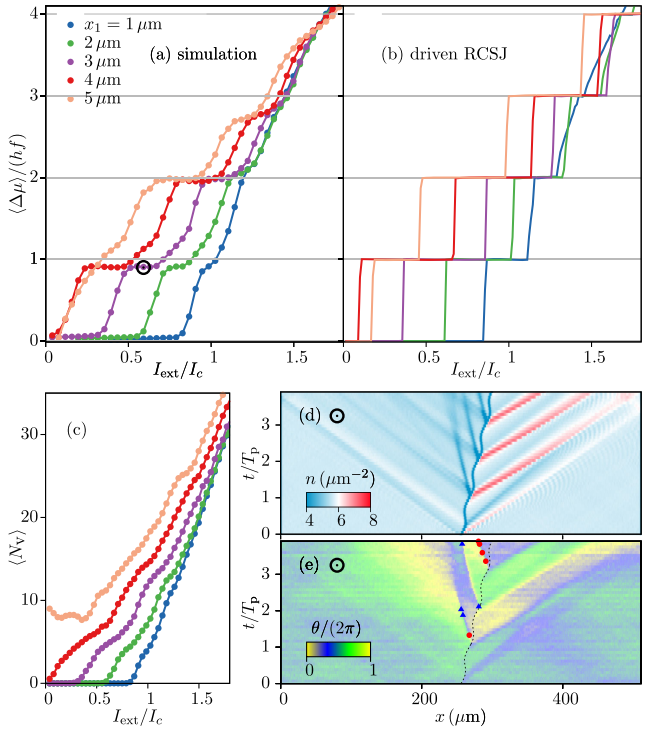


FIG. 3. Shapiro steps and the underlying vortex and phonon dynamics. (a) $\langle \Delta\mu \rangle$–$I_{\rm ext}$ response of the driven junction for $f/f_J = 2.2$ and $x_1 = 1$, 2, 3, 4, and 5 μm. The corresponding undriven junction with $\tilde{V}_0 = 1.5$ gives $I_c = 1.6 \times 10^5$ s$^{-1}$, $\hbar G = 157$, and the Josephson frequency $f_J = 25$ Hz. (b) Results of the driven RCSJ model shown for the same parameters as the simulations. (c) Time-averaged vortex number $\langle N_v \rangle$ corresponding to the simulations in (a). (d),(e) Time evolution of the density $n(x)$ and the phase $\theta(x, L_y/2)$ in the $x$ direction of the driven system at $I_{\rm ext}/I_c = 0.6$, which is indicated by the open circle symbol in (a). $T_p = 1/f$ is the driving period. $n(x)$ is averaged over the initial ensemble and the $y$ direction, whereas $\theta(x, L_y/2)$ represents the phase profile of a single sample. In (e), vortices (triangles) and antivortices (dots) are calculated using the phase change near the line at $L_y/2$ and the dotted line denotes the barrier motion.

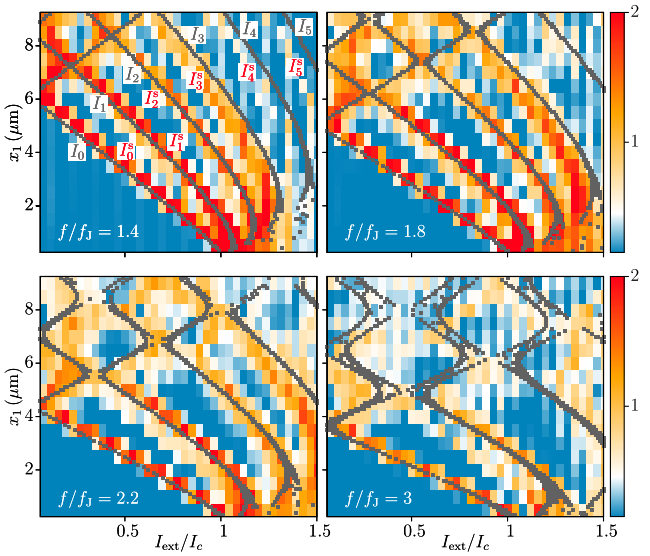


FIG. 4. Maximal current at the Shapiro steps. Differential resistance $d\mu/dI_{\rm ext}$ as a function of $I_{\rm ext}/I_c$ and $x_1$, for $f/f_J = 1.4$, 1.8, 2.2, and 3. The maxima of $d\mu/dI_{\rm ext}$ allow us to identify the maximal currents $I_0^s$, $I_1^s$, $I_2^s$, $I_3^s$, $I_4^s$, and $I_5^s$ of the Shapiro steps 0, 1, 2, 3, 4, and 5, respectively. The gray squares show the frequency and amplitude dependence of the maximal currents $I_k$ of the driven RCSJ model, determined using the same magnitude cutoff for all $f$, where the splitting of curve indicates a broadening of maxima. $k$ is the step index. We use $I_c = 1.6 \times 10^5$ s$^{-1}$, $f_J = 25$ Hz, and $\hbar G$ in the range 145–175, which are chosen according to the undriven system.

first step, whose onset and width feature an opposite trend than the corresponding results of low $x_1$ in Figs. 3(a) and 3(b). This occurs due to a Bessel-function type feature of the step width on $x_1$, which is evident from the results shown in Fig. 4. Even though $I_{\mathrm{ext}}$ is below $I_c$, as a consequence of the periodic driving, both density wave pulses in $n(x, y)$ and slippages of the local phase $\theta(x, y)$ near the barrier occur at the beginning of each driving cycle. Vortex formation and density waves are clearly correlated: vortex-antivortex pairs are generated that propagate behind the barrier; at the same time, density wave pulses of low velocity are observed in the left reservoir. Such phenomenon occurs in correspondence of the maxima, where the current near the barrier exceeds $I_c$, making the barrier effectively dissipative [53]; see Figs. 3(d) and 3(e).

To quantify the maximal current that develops at each step, we monitor the maxima $I_k^{\mathrm{s}}$ of the differential resistance $d\mu/dI_{\mathrm{ext}}$ at different driving frequencies. Figure 4 shows that the numerically obtained $I_k^{\mathrm{s}}$ follow the behavior of maximal currents of the driven RCSJ model. The amplitude of the peak decreases for both high steps and high driving frequencies, where the latter is partially captured by the driven model. The high-step damping originates from the depletion of the condensate density, which is a feature of the dynamics and does not affect the circuit model.

*Conclusions and outlook*—We have analyzed the time-averaged response of a driven atomic Josephson junction (JJ) at nonzero temperature. The JJ is created by separating two two-dimensional bosonic clouds with a tunneling barrier, where the barrier motion induces an external current and the periodic modulation of the barrier position acts as an external ac current drive. For the analysis, we employed classical-field simulations that capture the dynamics beyond mean field. The driven response demonstrates dc-ac transitions in the form of Shapiro steps. We compare these results with a driven RCSJ circuit model. Indeed, the steps result from resonances between the driving frequency $f$ and the periodic oscillations in the particle imbalance such that $\langle \Delta\mu \rangle = khf$, where $k$ is the step index. As a distinctive feature of our neutral superfluid system, the phenomenon arises from characteristic dynamics of vortex and phonon excitations. Our results can be directly probed, for example on ultracold $^6$Li machines employed in LENS [31] and Hamburg [30]. Because of the possibility to tune interactions from negative to positive values and relying on the know-how of the field allowing to work with bosonic and/or fermionic systems, spinor condensates [58], etc., Shapiro steps are expected to bear a great potential to explore the coherent properties of the artificial quantum matter as provided by cold atoms. Our results are important for both fundamental research in quantum dynamics of coherent systems and applications in quantum technologies.

*Acknowledgments*—We thank Giulia Del Pace, Giampiero Marchegiani, and Giacomo Roati for discussions. We acknowledge PHYSnet computing resources of University of Hamburg. L. M. acknowledges funding by the Deutsche Forschungsgemeinschaft (DFG) in the framework of SFB 925—project ID 170620586 and the excellence cluster "Advanced Imaging of Matter"—EXC 2056—project ID 390715994.

[1] B. D. Josephson, Possible new effects in superconductive tunnelling, Phys. Lett. **1**, 251 (1962).
[2] Rudolf Gross and Achim Marx, *Lecture Notes on Applied Superconductivity*, Chap. 3, pp. 89–113, https://www.wmi.badw.de/fileadmin/WMI/Lecturenotes/Applied_Superconductivity/AS_Chapter3.pdf.
[3] Sidney Shapiro, Josephson currents in superconducting tunneling: The effect of microwaves and other observations, Phys. Rev. Lett. **11**, 80 (1963).
[4] C. C. Grimes and Sidney Shapiro, Millimeter-wave mixing with Josephson junctions, Phys. Rev. **169**, 397 (1968).
[5] S. E. Hebboul, D. C. Harris, and J. C. Garland, Modulation of low–frequency shapiro steps of superconducting proximity-effect junctions, Physica (Amsterdam) **165-166B**, 1629 (1990).
[6] Daniel Rosenbach, Tobias W. Schmitt, Peter Schüffelgen, Martin P. Stehno, Chuan Li, Michael Schleenvoigt, Abdur R. Jalil, Gregor Mussler, Elmar Neumann, Stefan Trellenkamp, Alexander A. Golubov, Alexander Brinkman, Detlev Grützmacher, and Thomas Schäpers, Reappearance of first Shapiro step in narrow topological Josephson junctions, Sci. Adv. **7**, eabf1854 (2021).
[7] Shili Yan, Haitian Su, Dong Pan, Weijie Li, Zhaozheng Lyu, Mo Chen, Xingjun Wu, Li Lu, Jianhua Zhao, Ji-Yin Wang, and Hongqi Xu, Supercurrent, multiple Andreev reflections and Shapiro steps in InAs nanosheet Josephson junctions, Nano Lett. **23**, 6497 (2023).
[8] C. A. Hamilton, C. J. Burroughs, and R. L. Kautz, Josephson D/A converter with fundamental accuracy, IEEE Trans. Instrum. Meas. **44**, 223 (1995).
[9] C. J. Burroughs, S. P. Benz, T. E. Harvey, and C. A. Hamilton, 1 volt DC programmable Josephson voltage standard, IEEE Trans. Appl. Supercond. **9**, 4145 (1999).
[10] Charles J. Burroughs, Paul D. Dresselhaus, Alain Rufenacht, David Olaya, Michael M. Elsbury, Yi-Hua Tang, and Samuel P. Benz, NIST 10 V programmable Josephson voltage standard system, IEEE Trans. Instrum. Meas. **60**, 2482 (2011).
[11] O. Avenel and E. Varoquaux, Josephson effect and quantum phase slippage in superfluids, Phys. Rev. Lett. **60**, 416 (1988).
[12] E. Hoskinson, Y. Sato, I. Hahn, and R. E. Packard, Transition from phase slips to the Josephson effect in a superfluid $^4$He weak link, Nat. Phys. **2**, 23 (2006).
[13] S. Backhaus, S. V. Pereverzev, A. Loshak, J. C. Davis, and R. E. Packard, Direct measurement of the current-phase relation of a superfluid $^3$He-B weak link, Science **278**, 1435 (1997).
[14] J. C. Davis and R. E. Packard, Superfluid $^3$He Josephson weak links, Rev. Mod. Phys. **74**, 741 (2002).

[15] R. W. Simmonds, A. Marchenkov, J. C. Davis, and R. E. Packard, Observation of the superfluid shapiro effect in a $^3$He weak link, Phys. Rev. Lett. **87**, 035301 (2001).
[16] Luigi Amico, Gerhard Birkl, Malcolm Boshier, and Leong-Chuan Kwek, Focus on atomtronics-enabled quantum technologies, New J. Phys. **19**, 020201 (2017).
[17] L. Amico *et al.*, Roadmap on atomtronics: State of the art and perspective, AVS Quantum Sci. **3**, 039201 (2021).
[18] Luigi Amico, Dana Anderson, Malcolm Boshier, Jean-Philippe Brantut, Leong-Chuan Kwek, Anna Minguzzi, and Wolf von Klitzing, Colloquium: Atomtronic circuits: From many-body physics to quantum technologies, Rev. Mod. Phys. **94**, 041001 (2022).
[19] A. Ramanathan, K. C. Wright, S. R. Muniz, M. Zelan, W. T. Hill, C. J. Lobb, K. Helmerson, W. D. Phillips, and G. K. Campbell, Superflow in a toroidal Bose-Einstein condensate: An atom circuit with a tunable weak link, Phys. Rev. Lett. **106**, 130401 (2011).
[20] Stephen Eckel, Jeffrey G. Lee, Fred Jendrzejewski, Noel Murray, Charles W. Clark, Christopher J. Lobb, William D. Phillips, Mark Edwards, and Gretchen K. Campbell, Hysteresis in a quantized superfluid 'atomtronic' circuit, Nature (London) **506**, 200 (2014).
[21] C. Ryu, P. W. Blackburn, A. A. Blinova, and M. G. Boshier, Experimental realization of Josephson junctions for an atom SQUID, Phys. Rev. Lett. **111**, 205301 (2013).
[22] C. Ryu, E. C. Samson, and M. G. Boshier, Quantum interference of currents in an atomtronic SQUID, Nat. Commun. **11**, 3338 (2020).
[23] Chih-Chun Chien, Sebastiano Peotta, and Massimiliano Di Ventra, Quantum transport in ultracold atoms, Nat. Phys. **11**, 998 (2015).
[24] Sebastian Krinner, Tilman Esslinger, and Jean-Philippe Brantut, Two-terminal transport measurements with cold atoms, J. Phys. Condens. Matter **29**, 343003 (2017).
[25] F. S. Cataliotti, S. Burger, C. Fort, P. Maddaloni, F. Minardi, A. Trombettoni, A. Smerzi, and M. Inguscio, Josephson junction arrays with Bose-Einstein condensates, Science **293**, 843 (2001).
[26] L. J. LeBlanc, A. B. Bardon, J. McKeever, M. H. T. Extavour, D. Jervis, J. H. Thywissen, F. Piazza, and A. Smerzi, Dynamics of a tunable superfluid junction, Phys. Rev. Lett. **106**, 025302 (2011).
[27] G. Spagnolli, G. Semeghini, L. Masi, G. Ferioli, A. Trenkwalder, S. Coop, M. Landini, L. Pezzè, G. Modugno, M. Inguscio, A. Smerzi, and M. Fattori, Crossing over from attractive to repulsive interactions in a tunneling bosonic Josephson junction, Phys. Rev. Lett. **118**, 230403 (2017).
[28] Marine Pigneur, Tarik Berrada, Marie Bonneau, Thorsten Schumm, Eugene Demler, and Jörg Schmiedmayer, Relaxation to a phase-locked equilibrium state in a one-dimensional bosonic Josephson junction, Phys. Rev. Lett. **120**, 173601 (2018).
[29] Michael Albiez, Rudolf Gati, Jonas Fölling, Stefan Hunsmann, Matteo Cristiani, and Markus K. Oberthaler, Direct observation of tunneling and nonlinear self-trapping in a single bosonic Josephson junction, Phys. Rev. Lett. **95**, 010402 (2005).
[30] Niclas Luick, Lennart Sobirey, Markus Bohlen, Vijay Pal Singh, Ludwig Mathey, Thomas Lompe, and Henning Moritz, An ideal Josephson junction in an ultracold two-dimensional Fermi gas, Science **369**, 89 (2020).
[31] W. J. Kwon, G. Del Pace, R. Panza, M. Inguscio, W. Zwerger, M. Zaccanti, F. Scazza, and G. Roati, Strongly correlated superfluid order parameters from dc Josephson supercurrents, Science **369**, 84 (2020).
[32] S. Giovanazzi, A. Smerzi, and S. Fantoni, Josephson effects in dilute Bose-Einstein condensates, Phys. Rev. Lett. **84**, 4521 (2000).
[33] S. Levy, E. Lahoud, I. Shomroni, and J. Steinhauer, The a.c. and d.c. Josephson effects in a Bose–Einstein condensate, Nature (London) **449**, 579 (2007).
[34] G. Del Pace, W. J. Kwon, M. Zaccanti, G. Roati, and F. Scazza, Tunneling transport of unitary fermions across the superfluid transition, Phys. Rev. Lett. **126**, 055301 (2021).
[35] Antonio Barone and Gianfranco Paternò, High frequency properties and applications of the Josephson effect, in *Physics and Applications of the Josephson Effect* (John Wiley & Sons, Ltd, New York, 1982), Chap. 11, pp. 291–353.
[36] A. Burchianti, F. Scazza, A. Amico, G. Valtolina, J. A. Seman, C. Fort, M. Zaccanti, M. Inguscio, and G. Roati, Connecting dissipation and phase slips in a Josephson junction between fermionic superfluids, Phys. Rev. Lett. **120**, 025302 (2018).
[37] Vijay Pal Singh, Niclas Luick, Lennart Sobirey, and Ludwig Mathey, Josephson junction dynamics in a two-dimensional ultracold Bose gas, Phys. Rev. Res. **2**, 033298 (2020).
[38] K. Xhani, E. Neri, L. Galantucci, F. Scazza, A. Burchianti, K.-L. Lee, C. F. Barenghi, A. Trombettoni, M. Inguscio, M. Zaccanti, G. Roati, and N. P. Proukakis, Critical transport and vortex dynamics in a thin atomic Josephson junction, Phys. Rev. Lett. **124**, 045301 (2020).
[39] K. Xhani and N. P. Proukakis, Dissipation in a finite-temperature atomic Josephson junction, Phys. Rev. Res. **4**, 033205 (2022).
[40] Gabriel Wlazłowski, Klejdja Xhani, Marek Tylutki, Nikolaos P. Proukakis, and Piotr Magierski, Dissipation mechanisms in fermionic Josephson junction, Phys. Rev. Lett. **130**, 023003 (2023).
[41] A. Smerzi, S. Fantoni, S. Giovanazzi, and S. R. Shenoy, Quantum coherent atomic tunneling between two trapped Bose-Einstein condensates, Phys. Rev. Lett. **79**, 4950 (1997).
[42] S. Raghavan, A. Smerzi, S. Fantoni, and S. R. Shenoy, Coherent oscillations between two weakly coupled Bose-Einstein condensates: Josephson effects, $\pi$ oscillations, and macroscopic quantum self-trapping, Phys. Rev. A **59**, 620 (1999).
[43] Sigmund Kohler and Fernando Sols, Chemical potential standard for atomic Bose–Einstein condensates, New J. Phys. **5**, 94 (2003).
[44] André Eckardt, Tharanga Jinasundera, Christoph Weiss, and Martin Holthaus, Analog of photon-assisted tunneling in a Bose-Einstein condensate, Phys. Rev. Lett. **95**, 200401 (2005).

[45] Julian Grond, Thomas Betz, Ulrich Hohenester, Norbert J Mauser, Jörg Schmiedmayer, and Thorsten Schumm, The Shapiro effect in atomchip-based bosonic Josephson junctions, New J. Phys. **13**, 065026 (2011).
[46] C Ryu and M G Boshier, Integrated coherent matter wave circuits, New J. Phys. **17**, 092002 (2015).
[47] Halina Rubinsztein-Dunlop *et al.*, Roadmap on structured light, J. Opt. **19**, 013001 (2016).
[48] Daniel Barredo, Vincent Lienhard, Sylvain de Léséleuc, Thierry Lahaye, and Antoine Browaeys, Synthetic three-dimensional atomic structures assembled atom by atom, Nature (London) **561**, 79 (2018).
[49] M. J. Davis R. J. Ballagh P. B. Blakie, A. S. Bradley, and C. W. Gardiner, Dynamics and statistical mechanics of ultra-cold Bose gases using c-field techniques, Adv. Phys. **57**, 363 (2008).
[50] Anatoli Polkovnikov, Phase space representation of quantum dynamics, Ann. Phys. (Amsterdam) **325**, 1790 (2010).
[51] Vijay Pal Singh, Wolf Weimer, Kai Morgener, Jonas Siegl, Klaus Hueck, Niclas Luick, Henning Moritz, and Ludwig Mathey, Probing superfluidity of Bose-Einstein condensates via laser stirring, Phys. Rev. A **93**, 023634 (2016).
[52] Vijay Pal Singh and Ludwig Mathey, Sound propagation in a two-dimensional Bose gas across the superfluid transition, Phys. Rev. Res. **2**, 023336 (2020).
[53] See Supplemental Material at http://link.aps.org/supplemental/10.1103/PhysRevLett.133.093401 for the simulation method, the two-mode Gross-Pitaevskii equations, the estimate of the critical current, the ac dissipation mechanism, the scaling of characteristic parameters, and the time-averaged vortex number, which includes Refs. [31,32,37,43,54,55].
[54] Vinay Ambegaokar and Alexis Baratoff, Tunneling between superconductors, Phys. Rev. Lett. **11**, 104 (1963).
[55] F. Meier and W. Zwerger, Josephson tunneling between weakly interacting Bose-Einstein condensates, Phys. Rev. A **64**, 033610 (2001).
[56] Nikolay Prokof'ev, Oliver Ruebenacker, and Boris Svistunov, Critical point of a weakly interacting two-dimensional Bose gas, Phys. Rev. Lett. **87**, 270402 (2001).
[57] Nikolay Prokof'ev and Boris Svistunov, Two-dimensional weakly interacting Bose gas in the fluctuation region, Phys. Rev. A **66**, 043608 (2002).
[58] Bertrand Evrard, An Qu, Karina Jiménez-García, Jean Dalibard, and Fabrice Gerbier, Relaxation and hysteresis near Shapiro resonances in a driven spinor condensate, Phys. Rev. A **100**, 023604 (2019).